Fully Integrated Interferometry-Based Reflectometer for High-Impedance Instrumentation

Pietro Maris Ferreira, Cora Donche, Emilie Avignon-Meseldzija, Thomas Quémerais, Frederic Gianessello, Daniel Gloria, Tuami Lasri, Gilles Dambrine, Christophe Gaquière

Fully-Integrated Interferometry-Based Reflectometer for High-Impedance Instrumentation

Pietro Maris Ferreira, *Senior Member, IEEE*, Cora Donche, Emilie Avignon-Meseldzija, Thomas Quémerais, Frederic Gianesello, *Member, IEEE*, Daniel Gloria, Tuami Lasri, Gilles Dambrine, *Fellow Member, IEEE*, and Christophe Gaquière

***Abstract*—Microwave imaging of nanoelectronic devices has turned a simple reflection coefficient measurement, usually carried out by a 50 Ω vector-network analyzer (VNA), into a high impedance instrumentation challenge. Interferometry-Based Reflectometers (IBR) have been found to be successful solutions in addressing this challenge. However, such solutions do not consider instrumentation of high impedance and high-frequency as well as minimization of environment variations in a comprehensive manner. In this study, these aspects are addressed jointly through the proposal of a fully-integrated IBR in the STMicroelectronics BiCMOS 55 nm technology. Three varactor samples having a capacitance ranging from 0.65 fF to 0.95 fF are measured at 17.6 GHz for demonstration. The fully-integrated IBR achieved a magnitude error below -35 dB, a phase error below 0.03°, and an accuracy better than 59.7 aF. Moreover, C-V slope measurement error is better than 2.8 aF, which is ten times smaller than found in state-of-the-art IBR. Such betterment is explained by the monolithic integration of IBR and device-under-test (DUT) as implemented in this work.**

***Index Terms*—fully-integrated instrumentation, high-impedance microwave, Interferometry-Based Reflectometer, sub-fF MOS varactor, BiCMOS 55 nm**

I. Introduction

MICROWAVE imaging techniques remain a central topic for numerous medical, scientific, civil and military applications. They benefit from advanced 3D resolution thanks to a joint of topological information and electrical characteristics of a device-under-test (DUT). In the scientific field, scanning microwave microscopy (SMM) has an established setup mainly based on an Atomic Force Microscope (AFM) combined with a vector network analyzer (VNA). Using these techniques, different kind of properties (permittivity, conductivity) have been investigated from the measurement of the reflection coefficient of the DUT [1].

State-of-the-art systems are often developed using on the shelves devices. While its cost is undeniably low, such a solution also limits portability and very-large-scale integration. Against the tide of mainstream researches, M. Ruppert *et al* have presented a MEMS probe scanner using a SOI-MEMS fabrication process [2]. Ruppert's work presented a breakthrough in macroscale AFM systems towards fully-integrated SMM. Nevertheless, a challenge remains in microscale VNA based solution. In addition, SMM imaging of nanoelectronic devices has turned a simple reflection coefficient measurement, usually carried out by a 50 Ω VNA, into a high-impedance instrumentation problem in the bandwidth from 12 GHz to 18 GHz [3]. High-impedance microwave measurement challenges were highlighted in [1]. Such measurement techniques for nanoelectronic devices point out the difficulty in designing accurate reflectometers.

Towards a fully-integrated SMM, the authors have presented an Interferometry-Based Reflectometer (IBR) using transmission-based measurements [4]. Using a quite simple calibration technique, our previous work experimentally demonstrates IBR accuracy while measuring high-impedance microwave devices. Besides being a relatively cheap solution composed of a VNA and on the shelves devices, this transmission-based IBR is however not suitable for a fully-integrated SMM. A major reason for this is the large number of components (i.e. couplers, power splitters, and combiners). In addition to silicon-area costs, a fully-integrated transmission-based IBR would present significant performance variability and electromagnetic coupling noise, which turns out an impractical solution.

To manage the fully-integrated SMM challenges, a fully-integrated reflection-based IBR is proposed. To consider power and area constrains of a monolithic microwave integrated circuit, this work aims an all-passive IBR using a simpler topology compared to our previous work [4]. The fully-integrated IBR is proposed in the BiCMOS 55 nm technology for high-impedance microwave instrumentation of a DUT varactor varying from 0.65 fF to 0.95 fF. IBR measurement accuracy is compared with previous IBR using figures-of-merit introduced in [4]. Furthermore, fully-integrated IBR results are compared with the state-of-the-art of reflectometers using standard figures-of-merit proposed in [3]. In the perspective of a fully-integrated SMM, a fully-integrated cantilever using a MEMS probe as proposed in [2] and the fully-integrated IBR described here could be fabricated in a heterogeneous MEMS-CMOS process.

The rest of this paper is organized as follows. Section II reviews the state-of-the-art of reflectometers, highlighting reflection coefficient range and frequency of measurements. Section III describes the fully-integrated IBR based on reflection measurements, the calibration procedure, BiCMOS

The project received funding from the French Government and the Regional Council. This work has benefited of the facilities of ExCELSiOR-Nanoscience Characterization Center.

P. M. Ferreira and E. Avignon-Meseldzija are with GeePs, UMR CNRS 8507, CentraleSupélec, Université Paris-Saclay, Gif-sur-Yvette, France; email: maris@ieee.org. C. Donche, T. Lasri, G. Dambrine and C. Gaquière are with IEMN, UMR CNRS 8520, Lille 1 Univ., France. T. Quémerais, F. Gianesello, and D. Gloria are with STMicroelectronics, 850 rue Jean Monnet 38926 Crolles, France.

55 nm technology, and design considerations. Furthermore, post-layout simulations of the proposal are carried out; and DUT silicon-based modeling is described. Section IV presents fully-integrated IBR measurements and states a performance comparison between the proposal and the literature of reflectometers. Finally, paper conclusions are given in Section V.

II. Background

Abou-Khousa *et al.* have proposed a vector reflectometer using a narrow-band approach at 35.5 GHz [5], which is constituted of a controllable phase shifter and waveguides. The DUT reflection coefficient (Γ) magnitude and phase are obtained by solving a set of nonlinear equations at three or more phase shifts. The measurements were carried out using a short and a 3 mm offset short as DUTs, which achieves a $\Gamma \geq 0.99$.

Randus and Hoffmann have proposed an instrumentation method developed especially for high-impedance measurement (tens to hundreds of kΩ). Continuous wave measurements at 1.8 GHz were presented for a 2-port transmission-based interferometer for a DUT having a reflection coefficient $\Gamma = 0.999\angle -0.08^\circ$ [6]. Then, they have suggested a solution based on a 4-port port transmission-based interferometer including wideband measurements from 0.5 to 8 GHz of a dielectric resonator [7].

Laemmle *et al.* have presented a 125 GHz dielectric sensor with an integrated readout circuit [8]. The sensor has been used for the measurement of the dielectric constants of alcohols, whose a real and imaginary parts vary respectively from 5 to 4, and from 2 to 0.8. According to the authors, the absolute Γ is of minor interest, as the dielectric sensor presented is read out by phase differences.

Nasr *et al.* have proposed a one- and two-port fully integrated VNA using coherent detection, achieving an octave operational bandwidth from 50 GHz to 100 GHz [9]. The two-port VNA enables the measurement of the transmission parameter in one direction, working as a transmission-based reflectometer. The measurements were carried out using a V-band horn antenna $\Gamma \leq 0.1$.

Ferreira *et al.* have previously presented an IBR architecture associating a VNA and on the shelves devices [4]. Our previous reflectometer experimentally proved that IBR is an appropriate solution to measure sub-fF capacitance variations with a better accuracy than standard VNAs. Accurate measurements of varactors varying from 0.9 fF to 1.6 fF were achieved using a narrow-band approach at 6.8 GHz. However, our previous work proposed a transmission-based IBR which is not a practical solution when a fully-integrated implementation is envisaged.

A reflectometer for telecommunication was proposed by Hur and Eisenstadt [3]. Having a classical topology, the reflectometer is made of a power divider, a phase shifter, and power detectors. A large amount of measurement results was presented to experimentally demonstrate the reflectometer performance for 5G applications. Automated measurements were performed from 12 GHz to 18 GHz for a wide range of DUT reflection coefficient ($0.2 < \Gamma < 0.8$).

Staszek *et al.* have proposed a power distribution enhancing method in a reflectometer composed of power splitters and couplers [10]. Experimental verification of this enhanced power distribution technique was carried out for DUT reflection coefficient ($0.0001 < \Gamma < 0.6$) in the frequency band from 2.5 GHz to 3.5 GHz. From this solution, a significant improvement of the measurement accuracy in comparison to a classical reflectometer has been experimentally demonstrated.

In a similar architecture demonstrated in our previous work [4], Haddadi *et al.* have included an amplifier between the IBR and the VNA receiver to increase measurements sensitivity [11]. This work includes an amplification gain playing a role of imaging zoom, but the outcome of IBR complexity and power consumption increase. In fact, the primacy of this proposition goes to Randus and Hoffmann who have presented a complete theoretical and experimentally verified method to describe the amplifier role in the IBR [7]. Nevertheless, the amplifier non-idealities in terms of linearity and noise still must be investigated to assure negligible measurement sensitivity degradation in a fully-integrated IBR. For these reasons, this work is not included in following comparison.

Recently, Wessel et al. have presented a 120 GHz transmission-based interferometer for contactless permittivity measurements of biological materials [12]. In this work, a reconfigurable phase shifter using a slow wave line features with 256 switching states is proposed. This interferometer has respectively achieved resolutions of 0.09 and 0.0082° for the magnitude and the phase measured. However, as comparison data are not available for the material characterized in [12], this work is not included in following comparison.

Nehring *et al.* have proposed a miniaturized 4-32 GHz two-port VNA based on a fully integrated RF front-end (RX/TX) [13]. The system and receiver dynamic ranges were determined to be 44-77 and 82-101 dB at a resolution bandwidth of 100 kHz. Highly repeatable measurements were presented; and results are shown as robust against drift over time. Measurements were presented for a wide range of transmission coefficients and the full bandwidth, using a fixed coaxial attenuator with values ranging from 3 to 40 dB ($0.0001 \leq \Gamma \leq 0.5$).

III. Fully-Integrated Interferometry-Based Reflectometer

An Interferometry-Based Reflectometer (IBR), proposed in Fig. 1(a), is an instrumentation device based on a destructive-interference of reflection waves between a reference device (REF) and a tuner device (TUN). The device tuning operation is named nulling process and the resulting reflection coefficient is called Γ_{nil} [4]. The tuner is composed of an attenuator and a phase shifter to null the reference device reflection coefficient (equal magnitude and opposite phase shift). However, interference (INT) waves exist in any IBR instrument due to finite isolation in microwave devices (e.g. couplers, power dividers). In this case the electromagnetic wave results in a residue defined as

$$\Gamma_{nil} = \frac{\Gamma_{REF} + \Gamma_{TUN} + \Gamma_{INT}}{2}, \tag{1}$$

which can be simplified to

$$\Gamma_{nil} \approx \frac{\Gamma_{REF} + \Gamma_{TUN}}{2} \tag{2}$$

under the hypothesis that Γ_{INT} is negligible compared to Γ_{REF} and Γ_{TUN}. In fact, Γ_{INT} should be at least 20 dB below Γ_{REF} and Γ_{TUN} to guarantee such approximation. In this proposal, the reference device is a varactor fully-integrated with the IBR biased at -2.5 V. The proposed tuner device is a varactor fully-integrated in a Wilkinson power divider/combiner (Wilkinson PDC); and its design is described in Sec. III-B. During the nulling process Wilkinson power divider/combiner is tuned using a tuning voltage V_{TUN} until a specified Γ_{nil} is found ($\Gamma_{nil} \approx -65$ dB in this proposal). At this point is established a working frequency of the narrow-band reflectometer, named f_{nil}.

After the nulling process, a one-port vector calibration model is used [1]. Such method links the IBR reflection coefficient (Γ_{IBR} obtained at P1 in Fig. 1(a)) to the reflection coefficient of the device-under-test (Γ_{DUT} obtained at P2 in Fig. 1(a)). In this proposal, the device-under-test is a varactor fully-integrated with the IBR biased from -2.5 V to 2.5 V. Γ_{IBR} measurements are referenced to the high-impedance reference device ($\Gamma_{REF} = \Gamma_{DUT}$ for $V_{DUT} = -2.5$ V), while Γ_{DUT} measurements are referenced to a standard VNA (i.e. 50 Ω). One-port vector calibration method model is expressed by

$$\Gamma_{IBR} = E_{11} + \frac{E_{21}\Gamma_{DUT}}{1 - E_{22}\Gamma_{DUT}}. \tag{3}$$

The complex terms E_{11}, E_{21}, E_{22} can be calculated by solving the equation system from (3) using at least three known devices. To achieve a precise tracking-error modeling, known capacitors having a reflection coefficient close to the reference device should be chosen. In a fully-integrated demonstrator, replacing the DUT by known capacitors is however not an option since DUT and IBR are physically connected. To overcome such limitation, the proposed tunable Wilkinson PDC is integrated in a different footprint. Scattering parameters of the tunable Wilkinson PDC are measured using a standard procedure with a calibrated VNA. From the tunable Wilkinson PDC measurements and RF connections modeling a post-measurement IBR model is obtained using ADS. Thus, the proposed IBR model is used instead in one-port vector calibration. Obtained one-port vector calibration model will be valid in a logarithmic-domain capacitance of a linear IBR model, assuming root mean square model error lower than 5 % (see Sec IV).

Knowing these tracking-errors, one can obtain the Γ_{DUT} of any unknown device from measured Γ_{IBR}. In this work, a sub-fF varactor is chosen as the unknown DUT. The capacitance value is modified using a control voltage named V_{DUT}. Taking losses into account, capacitance measurements are given by

$$C_{DUT} = -\frac{Re(Y_{DUT})^2 + Im(Y_{DUT})^2}{2\pi \cdot f_{nil} \cdot Im(Y_{DUT})}, \tag{4}$$

where Y_{DUT} is obtained from Γ_{DUT}, after applying tracking-error model previously obtained.

A. Technology description

The circuit was fabricated in the BiCMOS SiGe 55 nm technology. This technology, developed by STMicroelectronics, is dedicated to millimeter wave (mmW) and sub-mmW applications. For instance, a SiGe bipolar transistor with 0.2 μm emitter width presents a frequency ratio f_T/f_{MAX} of 320/370 GHz [14] for a collector current density of 16 mA/μm^2.

This technology includes 8 metal levels, in addition of a top copper metal layer of 3 μm thick. Moreover, the 55 nm technology offers an accumulation MOS varactors dedicated to mmW applications ($f_{osc} > 110$ GHz). This enables the integration of passive RF components like inductors, transmission lines and MOS varactors with good quality factors. Measured Q-factors larger than 10 are obtained at mmW frequencies [14].

B. Design Considerations

The device block-diagram (see Fig. 1(a)) is composed of an external VNA (Agilent PNA - E8363B), a tunable Wilkinson PDC, and a varactor. Such varactor will play a role of reference device (biased at $V_{DUT} = -2.5$ V) during nulling process and a role of device-under-test (biased as $-2.5\text{V} \leq V_{DUT} \leq 2.5$ V) during IBR measurements (see Sec. IV). Only magnitude nulling was integrated in the fully-integrated IBR demonstrator. One can mention that phase nulling is an additional degree of freedom to select a specific frequency for Γ_{nil} in narrow-band IBR [1]. To that end, the fully-integrated IBR should include a tunable phase shifter inserted between the port P3 and the short-circuit (see Fig. 1(a)) to allow phase nulling. However, phase nulling is out of the scope of this work.

Fig. 1(b) presents the micro-photography of the proposed IBR. Fully-integrated IBR chip size is 243 x 216 μm^2. Additional area is required for demonstrator micro-strip lines and PADs, which are not considered as part of IBR core. RF port P1 was designed to fit a microprobe MPI Infinity, 50 GHz, GSG, 100 μm pitch. P3 is physically shorted to ground plane while P2 is connected to a sub-fF varactor (DUT). V_{DUT} and V_{TUN} are DC voltages varying from -2.5 V to 2.5 V. Such DC voltages are controlled through single-DC microprobes using Keysight (Agilent) IC-CAP device modeling software.

The integrated tunable Wilkinson PDC is depicted in Fig. 1(c). Such block is based on passive lumped elements, having a tunable characteristic set by V_{TUN}. During the nulling process, such block should achieve a directivity of at least 20 dB (i.e. $D \geq 20$ dB) to guarantee a negligible Γ_{INT}, with the directivity defined as:

$$Directivity = -S_{32} - (S_{31} + S_{21}). \tag{5}$$

By choosing a proper V_{TUN}, the directivity is maximized. Under this condition, the wave power in the path S_{32} is strongly attenuated by an increasing $C_{TUN} + C_1$ over V_{TUN}. Besides, Γ_{REF} and Γ_{DUT} waves shall be matched with a small as possible attenuation according to (2). To this end, it is required a minimum $S_{21} = S_{31}$. Thus, a destructive interference between the reflected waves (REF and DUT) takes place and a Γ_{nil} at f_{nil} is found.

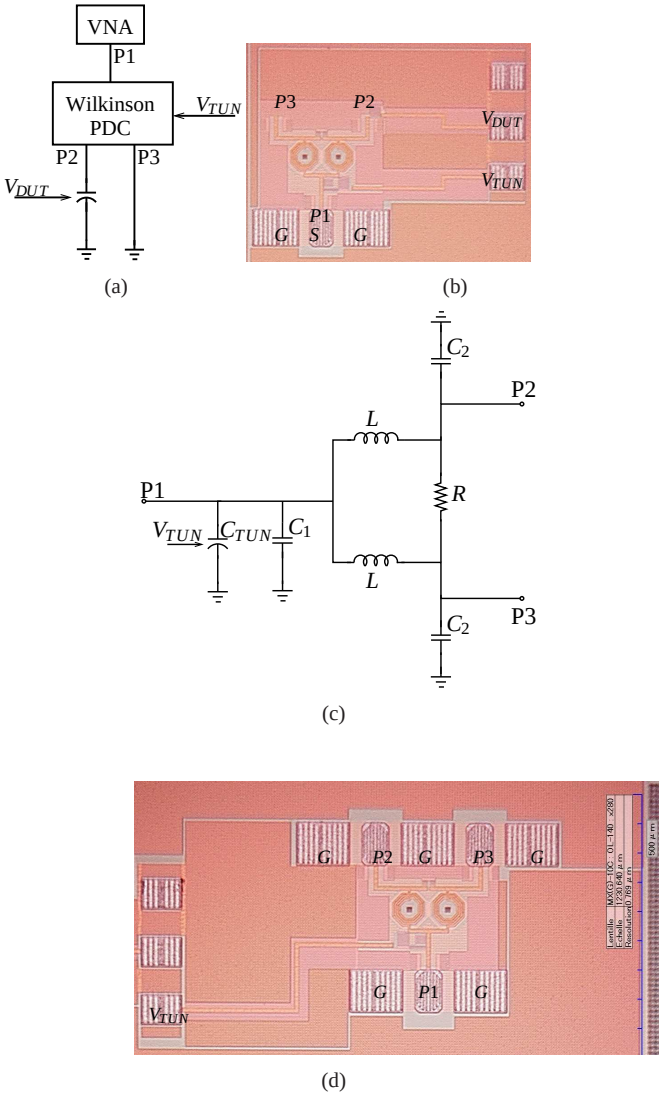

Fig. 1. Interferometry-Based Reflectometer: illustration of (a) IBR block diagram; (b) IBR microchip photograph; (c) Wilkinson PDC schematic; and (d) Wilkinson PDC microchip photograph . Tuning (V_{TUN}) and DUT (V_{DUT}) control voltages vary from -2.5 V to 2.5 V.

In order to provide the directivity tuning possibility to a lumped Wilkinson PDC, one could change inductance or capacitance values (see Fig. 1(c)). In this work, the choice has been made to vary the capacitance value by using high-quality-factor thick oxide accumulation MOS varactors. A simulation-based design methodology permits to find an optimal value of C_2 considering that it will be in parallel to C_{DUT} at port P2 and in short-circuit at P3. Thus, only C_1 is designed to be reconfigurable by a parallel association of a Metal-Insulator-Metal (MIM) capacitor C_1 and a varactor C_{TUN}. A tunable Wilkinson PDC was optimized using ADS software (Agilent), and device sizing is presented in Table I. Fig. 1(d) presents the micro-photography of the tunable Wilkinson PDC integrated in a separate footprint.

TABLE I
TUNABLE WILKINSON PDC DESCRIPTION

Device	Value	Device	Value
R	150.93 Ω	L	707.1 pH
C_1	188 fF	C_2	140.9 fF
C_{TUN}	[65 fF,95 fF]	C_{DUT}	[0.65 fF,0.95 fF]

C. Post-Layout Simulations

IBR's post-layout simulations consider the ADS measurement models offered by the 55 nm process design kit, which includes lumped elements, micro-strip lines and PADs. To obtain an accurate model of the IBR, an ideal capacitor (C_{ideal}) is used instead of a varactor (C_{DUT}) for the nulling process automation. Fig. 2 highlights the IBR nulling process (assuming (2)) for a $C_{ideal} = 10$ aF achieving a $\Gamma_{nil} = -99$ dB at $f_{nil} = 15.77$ GHz for $V_{TUN} = -0.3$ V.

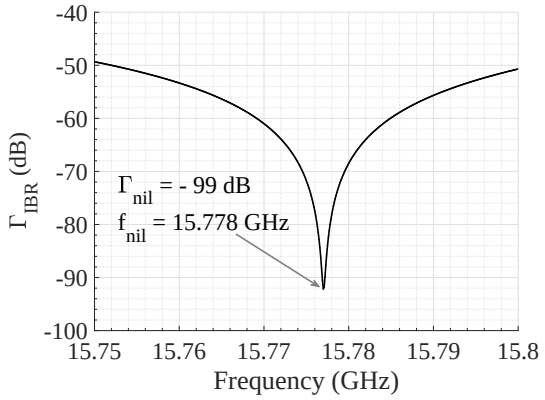

Fig. 2. Post-Layout simulations of IBR nulling process (assuming (2)) for an ideal $C_{DUT} = 10$ aF for $V_{TUN} = -0.3$ V.

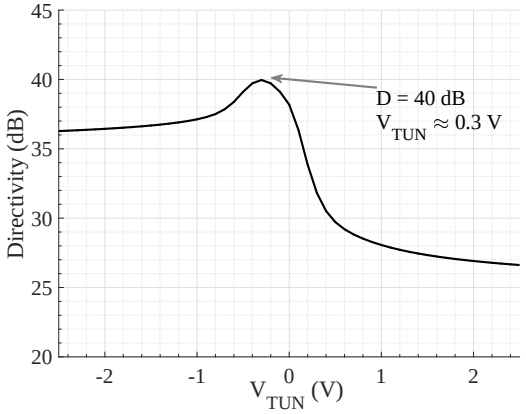

Fig. 3. Post-Layout simulations of Wilkinson PDC directivity (see (5)) at f_{nil}, a maximum of 40 dB is found for $V_{TUN} \approx -0.3$ V.

As illustrated in Fig. 3, the tunable Wilkinson PDC directivity (see (5)) reaches a maximum of 40 dB at $V_{TUN} \approx -0.3$ V. A priori knowledge of directivity as a function of nulling frequency and V_{TUN} is desired to minimize Γ_{nil} (see Subsec III-B). Measurement automation is also favored by a precise control of the Wilkinson PDC directivity tuning.

D. 55 nm MOS varactor silicon-based modeling

The varactor is a thick oxide, accumulation MOS varactor using subdesign-rules channel with a minimum gate length of 55 nm. This increases greatly its quality factor especially at millimeter-wave frequencies. A T-cell model (Fig. 4) is used in order to take into account all the varactor physical elements including substrate parameters. The silicon-based model presented by T. Quemérais *et al.* in [15] is scalable for all varactors dimensions: gate finger length (l), gate finger width (w), number of gate finger (N) and the number of devices in parallel ($Mult$).

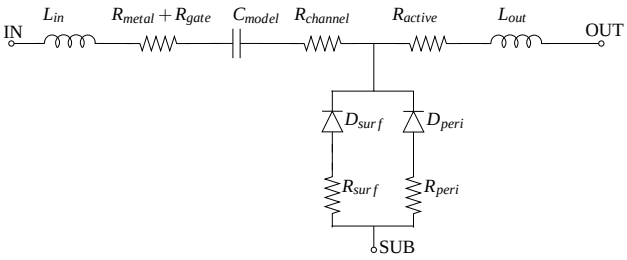

Fig. 4. Equivalent electrical circuit of the varactor.

In Fig. 4, C_{model} is given by the relationship

$$C_{model} = \frac{1}{\frac{1}{C_{ox}(w,N,l)} + \frac{1}{C_{sc}(w,N,l)}} + C_{metal}(w,N,l) + C_{peri}(w,N,l). \quad (6)$$

C_{metal} is the metal-interconnection parasitic, dependent on the geometrical and physical dimensions of the varactor. C_{peri} is the perimeter-fringe parasitic, mainly dependent on the varactor finger gate perimeter dimensions. The voltage dependent MOS capacitance is equivalent to semiconductor (C_{sc}) and oxide (C_{ox}) capacitances. Both C_{sc} and C_{ox} are based on the BSIM 4 compact model with specific fitting parameters [15]. Varactor modeling (see Fig. 4) considers losses of: R_{metal} (metal access resistance), R_{gate} (polysilicon gate resistance), $R_{channel}$ (voltage dependent channel resistance), and R_{active} (active P+ resistances).

The series inductances L_{in} and L_{out} model respectively the metal interconnections input and output accesses of the varactor as a function of its dimensions. The varactor substrate Nwell-Pwell is modeled by a perimeter diode (D_{peri}) and a surface diode (D_{surf}). In Fig. 4, substrate resistances R_{peri} and R_{surf} represent perimeter and surface resistance of N- and P-well. This model enables to accurately simulate varactors behavior up to millimeter wave frequencies for all geometries. To achieve the desired capacitance variation (i.e. from 0.65 fF to 0.95 fF), the DUT sizing is $l = 55$ nm, $w = 1.4$ μm, $N = 1$, and $Mult = 1$.

IV. Measurements

Three different samples of the proposed fully-integrated IBR were chosen to demonstrate instrument performance. For each sample (named A, B and C), the nulling process was carried out by measuring Γ_{nil} with an external VNA, while V_{TUN} is varied. The nulling process is ended achieving a $\Gamma_{nil} \leq -65$ dB for $V_{TUN} = 0.1$ V. To achieve a precise nil, an averaging of 16-points is employed in VNA configuration.

Fig. 5 depicts the nulling process result for sample A. Similar results are found for samples B and C. The proposed fully-integrated IBR achieves a $f_{nil} = 17.58$ GHz. Post-layout simulations estimated a $f_{nil} = 15.77$ GHz (see Fig. 2). This difference can be attributed to the imprecision in the fabrication of passive components (i.e. inductors in Wilkinson PDC). Such components mismatch (process variability) can be explained by measuring the Wilkinson PDC from a separate block using a VNA. To understand such limitation, the proposed tunable Wilkinson PDC is integrated in a different footprint illustrated in Fig.1(d). Scattering parameters of the tunable Wilkinson PDC are measured using a standard procedure with a calibrated VNA (Agilent PNA - E8363B). Fig. 6 shows the Wilkinson PDC directivity (see (5)) at $V_{TUN} \approx 0.1$ V. Among all three samples, the required condition for the directivity ($D \geq 20$ dB) is found from 17 to 18 GHz, whereas such condition is found from 14.5 to 16.5 GHz for post-layout simulations. One can observe that the value of f_{nil} is strongly dependent of phase mismatch between ports P2 and P3. This result demonstrates that phase configuration is an important degree of freedom to exploit if a specific f_{nil} is required. Nevertheless, f_{nil} reconfiguration is out of the scope of this work.

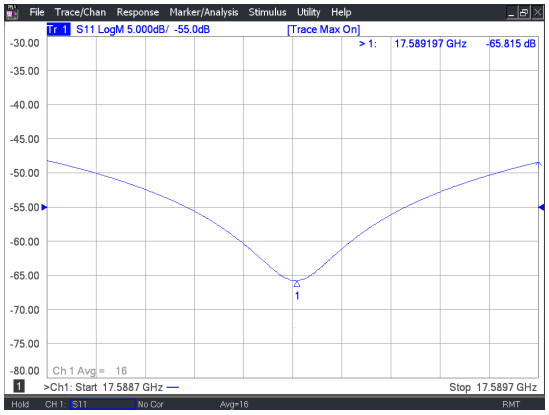

Fig. 5. IBR Nulling procedure for sample A: Tuning of the reflection coefficient at -65 dB at 17.58 GHz for $V_{TUN} = 0.1$ V.

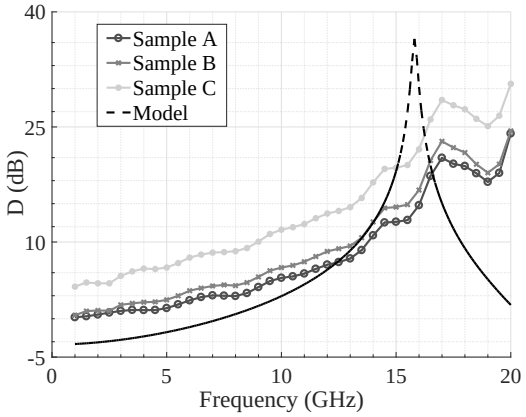

Fig. 6. Wilkinson PDC measured directivity at $V_{TUN} \approx 0.1$ V, which is used to build the post-measurement IBR model.

Following the nulling process, a one-port vector calibration method is carried out for each sample by solving (3). A calibration correction procedure should be verified by measuring a significantly different and traceable standard kits. However, the fully-integrated demonstrator investigated cannot be calibrated this way as both DUT and IBR are physically integrated in a single device. To overcome such characteristics, it is proposed here to use as an alternative the post-measurement modeling presented in Fig. 7 for one-port vector calibration method model. A post-measurement IBR model is simulated using ADS and an extracted model of the Wilkinson PDC from results of Fig. 6. Post-measurement simulations are obtained for a wide range of ideal capacitance values from 20 aF to 100 fF. As shown in Fig. 7, P1 reflection wave Γ_{IBR} after nulling process has a linear dependence in a logarithmic-domain DUT capacitance for $C_{ideal} \geq 0.1$ fF. According to a linear regression fitting applied to Γ_{IBR} in dB as a function of a logarithmic-domain C_{ideal}, the proposed post-measurement IBR model achieves a root mean square error lower than 5 % from 0.5 fF to 3 fF. As in this work, the IBR demonstrator is integrated using a varactor C_{DUT} varying from 0.65 fF to 0.95 fF; one can argue that the IBR is operated in linear regime. From this modeling, a one-port vector calibration method is carried out for three capacitance values of 0.73 fF, 0.8 fF, and 0.88 fF. Such capacitance has a Γ_{IBR} equals to respectively -48.3 dB, -47.5, and -46.7 dB according to post-measurement IBR model (see Fig. 7). Such capacitors are chosen close to the nulling reference minimizing IBR tracking errors for such instrumentation conditions.

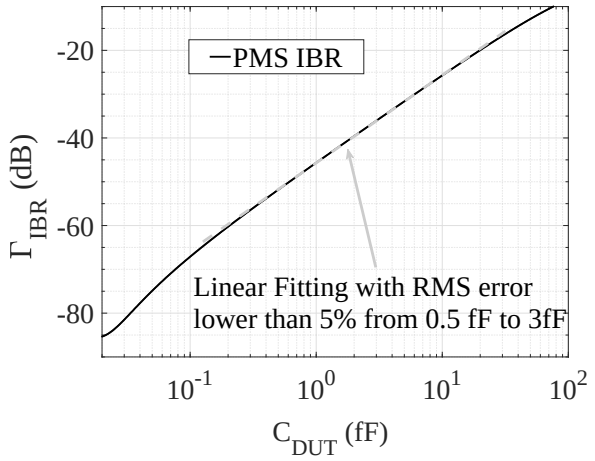

Fig. 7. Interferometry-Based Reflectometer: Post-measurement simulations of P1 reflection coefficient Γ for $C_{ideal} \in [20\ aF, 100\ fF]$ variation using an extracted model of the Wilkinson PDC (see Sec. IV).

Device-under-test capacitance values were measured for $V_{DUT} \in [-2.5\text{ V}, 2.5\text{ V}]$, while $C_{DUT} \in [0.65\ fF, 0.95\ fF]$. Sub-fF MOS varactor instrumentation of samples A, B, and C are obtained from Γ_{DUT} referenced to 50 Ω (after error-tracking model) by (4). As high-impedance measurements using a VNA are less accurate than those achieved by using interferometer-based reflectometer [4], measurement results are compared to varactor silicon-based modeling presented in Subsection III-D.

Fig. 8 shows the C-V curves for silicon-based model and IBR samples (A, B, and C). The fully-Integrated demonstrator has presented a remarkable accuracy, which is evaluated by [4]

$$RMSE_i = \sqrt{mean\left((C_i - C_{model})^2\right)}. \tag{7}$$

Demonstrator samples have presented a $RMSE_A = 44.3\ aF$, $RMSE_B = 59.7\ aF$, and $RMSE_C = 34.8\ aF$. A $RMSE_{IBR} = 60$ aF was obtained in our previous work [4]. Betterments brought by the fully-integrated solution are due to $C_{REF} \approx C_{DUT}$ during the nulling process and to accurate error-tracking model using capacitance values close to C_{DUT}. Besides, fully-integrated IBR minimizes losses between connections and losses due to environment variation thanks to compact integration.

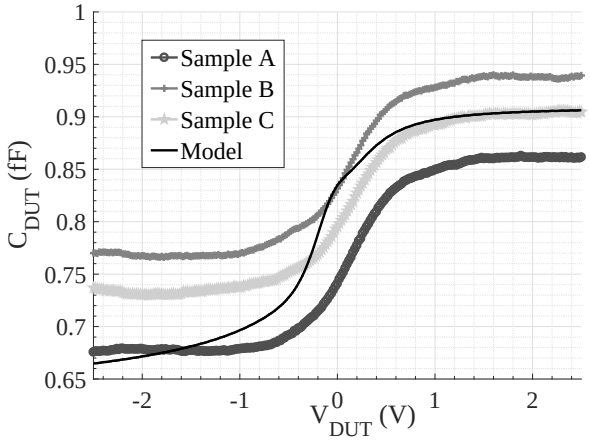

Fig. 8. Sub-fF MOS varactor instrumentation: C-V curves using silicon-based model, and IBR samples (A,B, and C).

In addition, a figure-of-merit [4]

$$\alpha_i = \sqrt{mean\left((\Delta C_i - \Delta C_{model})^2\right)} \tag{8}$$

is considered to compare sub-fF C-V slope of the proposed fully-integrated IBR with our previous work. Fully-Integrated demonstrator samples have presented a $\alpha_A = 1.12\ aF$, $\alpha_B = 1.17\ aF$, and $\alpha_C = 1.14\ aF$, while a $\alpha_{IBR} = 11$ aF has been previously obtained [4]. This result experimentally confirms that interferometer-based reflectometer strengths in measuring small Γ variation in high-impedance instrumentation are even more enhanced in fully-integrated solution.

Most of reflectometers described in the literature focus on precise measurements of lesser reflective devices. They usually compare reflectometer (Γ_R) to VNA (Γ_{VNA}) measurements by figures-of-merit:

$$\text{Magnitude Error } = |\Gamma_R - \Gamma_{VNA}|, \text{ and} \tag{9}$$

$$\text{Phase Error } = \angle\Gamma_R - \angle\Gamma_{VNA}. \tag{10}$$

Since users of classic reflectometers are not interested in measuring Γ variation, only absolute errors are found in the literature. To compare the proposed IBR to the state-of-the-art of reflectometers, absolute errors given by (9) and (10) were determined. However, in high-impedance instrumentation Γ_{VNA} exhibits the impedance mismatch stated in [1] and

experimentally proved in [4] To evaluate our results against the literature, a straight forward comparison is difficult to make directly. Hence, the VNA measurements (Γ_{VNA}) used as a reference are replaced by silicon-based model (Γ_{model}) (described in Subsec. III-D) in (9) and (10).

Table II reveals that Staszek's reflectometer [10] has the smallest magnitude error, but also a big phase error. A smaller phase error is observed in solutions measuring highly-reflective devices as for Abou-Khousa's proposal [5], however only two different Γ were measured. Fully-integrated VNAs have presented either low phase error of 0.3° [9] and 0.082° [8] or low magnitude error of -36 dB [13]. The fully-integrated IBR has presented the smallest phase error (below 0.03°) among literature reflectometers and smaller magnitude error than our previous IBR [4]. Phase error performance is explained by the own nature of interferometer-based measurements, which can accurately estimate Γ variations by observing Γ phase [1]. Besides, magnitude errors might be lowered when using an amplification gain as demonstrated in [6]. Regardless, amplifier non-idealities must be investigated to assure a negligible measurement sensitivity degradation in a fully-integrated IBR.

TABLE II
REFLECTOMETER PERFORMANCE COMPARISON

Ref.	Freq. (GHz)	DUT characteristics	Mag. Error (dB)	Phase Error (°)
This Work	17.8	$0.65 < C(\text{fF}) < 0.95$	-35 (A) -33 (B) -39 (C)	0.02 (A) 0.03 (B) 0.01 (C)
[13]	4-32	$0.0001 < \Gamma < 0.5$	-36	3.23
[10]	2.5-3.5	$0.0001 < \Gamma < 0.6$ $0 < \angle\Gamma(^\circ) < -90$	-48	2.63
[3]	15-18	$0.2 < \Gamma < 0.8$ $30 < \angle\Gamma(^\circ) < 330$	-30	5
[4]	6.8	$0.9 < C(\text{fF}) < 1.6$	-32 (IBR) -34 (VNA)	0.18 (IBR) 0.2 (VNA)
[9]	50-100	$0.001 < \Gamma < 0.1$	-30	0.3
[8]	121	$\Gamma = 0.41, 0.34$ $\angle\Gamma(^\circ) = -11.3, -7.3$	NA	0.082
[6]	1.8	$\Gamma = 0.999\angle -0.08^\circ$	-43 (min) -31 (max)	0.11 (min) 0.72 (max)
[5]	35.5	$\Gamma = 0.9968, 0.9977$ $\angle\Gamma(^\circ) = 25.83, -179.97$	-33	0.2

V. CONCLUSIONS

A fully-integrated IBR is proposed in this work. IBR operation and design considerations are presented. Measurement results are shown for 55 nm MOS varactors varying from 0.65 fF to 0.95 fF at 17.8 GHz. The ability in measuring accurately high-impedance microwave devices was demonstrated using literature figures-of-merit. Compared to reflectometers found in literature, the proposed IBR shows the smallest phase error (below 0.03°) and small enough magnitude error. Compared to our previous work the IBR accuracy *RMSE* (lower than 59.7 aF) is in the same order (i.e. 60 aF), but the C-V slope measurement error α (lower than 1.17 aF) is ten times smaller than the one formerly observed. Such betterment is explained by the monolithic integration of both IBR and DUT.

REFERENCES

[1] H. Happy, K. Haddadi, D. Théron, T. Lasri, and G. Dambrine, "Measurement Techniques for RF Nanoelectronic Devices," *IEEE Microw. Mag.*, vol. 15, no. 1, pp. 30–39, 2014.

[2] M. G. Ruppert, A. G. Fowler, M. Maroufi, and S. O. R. Moheimani, "On-Chip Dynamic Mode Atomic Force Microscopy : A Silicon-on-Insulator MEMS Approach," *J. Microelectromech. Syst.*, vol. 26, no. 1, pp. 215–225, Feb 2017.

[3] B. Hur and W. R. Eisenstadt, "Automated Wideband Test System , Measurement Uncertainty , and Design of On-chip Six-Port Reflectometers for 5G Applications," in *Proc. IEEE Microw. Meas. Conf. (ARFTG)*, Philadelphia, PA, USA, Jun 2015.

[4] P. M. Ferreira *et al.*, "Sub-fF 130 nm MOS Varactor Characterization using 6.8 GHz Interferometry-based Reflectometer," *IEEE Microw. Compon. Lett*, vol. 25, no. 6, pp. 418–420, Jun 2015.

[5] M. A. Abou-Khousa, M. a. Baumgartner, S. Kharkovsky, and R. Zoughi, "Ka-band vector reflectometer based on simple phase-shifter design," *IEEE Trans. Instrum. Meas.*, vol. 60, no. 2, pp. 618–624, Feb 2011.

[6] M. Randus and K. Hoffmann, "Microwave impedance measurement for nanoelectronics," *Radioengineering*, vol. 20, no. 1, pp. 276–283, Apr 2011.

[7] M. Randus and K. Hoffmann, "A method for direct impedance measurement in microwave and millimeter-wave bands," *IEEE Trans. Microw. Theory Techn.*, vol. 59, no. 8, pp. 2123–2130, Aug 2011.

[8] B. Laemmle, K. Schmalz, J. C. Scheytt, R. Weigel, and D. Kissinger, "A 125-GHz permittivity sensor with read-out circuit in a 250-nm SiGe BiCMOS technology," *IEEE Trans. Microw. Theory Techn.*, vol. 61, no. 5, pp. 2185–2194, May 2013.

[9] I. Nasr, J. Nehring, K. Aufinger, G. Fischer, R. Weigel, and D. Kissinger, "Single-and dual-port 50-100-GHz integrated vector network analyzers with on-chip dielectric sensors," *IEEE Trans. Microw. Theory Techn.*, vol. 62, no. 9, pp. 2168–2179, Sep 2014.

[10] K. Staszek, S. Gruszczynski, and K. Wincza, "Six-Port Reflectometer Providing Enhanced Power Distribution," *IEEE Trans. Microw. Theory Techn.*, vol. 64, no. 3, pp. 939–951, Jan 2016.

[11] K. Haddadi, C. Brillard, G. Dambrine, and D. Théron, "Sensitivity and Accuracy Analysis in Scanning Microwave Microscopy," in *IEEE MTT-S Int. Microw. Symp. (IMS)*, San Francisco, CA, USA, May 2016, pp. 1–4.

[12] J. Wessel, K. Schmalz, J. C. Scheytt, and D. Kissinger, "A 120-GHz Electrical Interferometer for Contactless Permittivity Measurements with Direct Digital Read-Out," *IEEE Microw. Compon. Lett.*, vol. 27, no. 2, pp. 198–200, Feb 2017.

[13] J. Nehring, M. Schutz, M. Dietz, I. Nasr, K. Aufinger, R. Weigel, and D. Kissinger, "Highly Integrated 4-32-GHz Two-Port Vector Network Analyzers for Instrumentation and Biomedical Applications," *IEEE Trans. Microw. Theory Techn.*, vol. 65, no. 1, pp. 229–244, Jan 2017.

[14] P. Chevalier *et al.*, "A 55 nm triple gate oxide 9 metal layers SiGe BiCMOS technology featuring 320 GHz f_T / 370 GHz f_{MAX} HBT and high-Q millimeter-wave passives," in *Int. Electron Devices Meeting, IEDM*, San Francisco, CA, USA, Dec. 2014, pp. 3.9.1–3.9.3.

[15] T. Quémerais, D. Gloria, D. Golanski, and S. Bouvot, "High-Q MOS Varactors for Millimeter-Wave Applications in CMOS 28 nm FDSOI," *IEEE Electron Devices Lett.*, vol. 36, no. 2, pp. 87–89, Feb 2015.

Pietro Maris Ferreira (S'03-SG'06-M'12-SM'18) received the B.Sc. cum lauda and the M.Sc. degrees from the Federal University of Rio de Janeiro (UFRJ), Brazil in 2006 and 2008, respectively; and the Ph.D. degree from the Télécom ParisTech, France, in 2011, all in electronic engineering. Researching high-performance high-reliability circuits and systems, he joined IM2NP lab. (UMR CNRS 7334) for one year and IEMN lab. (UMR CNRS 8520) for two years during his tenure track. Since 2014, he has been with GeePs lab. (UMR CNRS 8507) as Associate Professor of the Dep. of Electronic Systems of CentraleSupélec at Université Paris-Saclay.

Cora Donche received the B.S. and M.S. degrees in microelectronics and nanotechnologies from the University of Lille, France, in 2011. She joined CEA-Leti from 2011 to 2013 as instrumentation engineer; and IEMN lab. (UMR CNRS 8520) from 2013 to 2015 as research engineer. Nowadays, she is with SADTEM as instrumentation engineer. Her principal interests are device modeling and electrical characterization.

Emilie Avignon-Meseldzija received in 2004 the Master degree in Electronics from the Pierre et Marie Curie University, France and the PhD degree from the same university in 2007. In 2007, she joined GeePs lab. (UMR CNRS 8507) as Associate Professor of the Dep. of Electronic Systems of CentraleSupélec at Université Paris-Saclay. Her fields of interest are mainly electronics dedicated to radar applications and circuits for analog signal processing.

Thomas Quémerais was born in Guérande, France, on May 1982. He received the M.S. and PhD degree in Physics of Semiconductors and Microwaves from the Grenoble Institute of Technology (INPG), France in 2007 and 2010. His doctoral research was in electrical characterization, modeling and reliability study of RF and millimeter-wave passive and active circuit in SiGe BiCMOS and advanced CMOS technologies. Since 2010, he is with STMicroelectronics, Crolles, France. His principal research interests are in the RF and millimeter wave silicon device modeling and electrical characterization. Since 2016, he is with STMicroelectronics, Grenoble, Imaging Division, France. His principal research interests are in the pixel control analog design.

Frederic Gianesello (M'13) received the B.S. and M.S. degrees in electronics engineering from the Institut National Polytechnique de Grenoble, Grenoble, France, in 2003 and the Ph.D. degree in electrical engineering from the Joseph Fourier University, Grenoble, France, in 2006.

He is currently working for STMicroelecetronics, Crolles, France, where he leads the team responsible for the development of electromagnetic devices (inductor, balun, transmission line, and antenna) integrated on advanced RF CMOS/BiMOS (down to 14 nm), silicon photonics, and advanced packaging technologies (3-D Integration, FOWLP, etc.). He has authored and coauthored more than 110 refereed journal and conference technical articles. Dr. Gianesello has served on the TPC for the International SOI Conference from 2009 up to 2011 and he is currently serving on the TPC for the Loughborough Antennas and Propagation Conference (LAPC).

Daniel Gloria received the Engineering degree in electronics from the Ecole Nationale Superieure d'Electronique et de Radioelectricité, Grenoble, France, in 1995, and the M.S.E.E. degree in optics, optoelectronics, and microwave design systems from the National Polytechnic Institute of Grenoble, Grenoble, in 1995. From 1995 to 1997, he was a Radio Frequency (RF) Design Engineer with ALCATEL Bell Network System Laboratories, Charleroi, Belgium, where he was involved in the development of the cable phone RF front ends and their integration in hybrid-fiber-coax telecommunication networks. Since 1997, he has been with Central Research and Development, STMicroelectronics, Crolles, France, as a High-Frequency (HF) Research Engineer. His current research interests include optimization of active and passive devices for HF applications in BiCMOS and CMOS advanced technologies.

Tuami Lasri has been involved in studies in energy with the development of microgenerators based on thermoelectric transduction. He is currently a Professor of Electronics and Electrical Engineering with the University of Lille 1, Villeneuve d'Ascq, France. His current research interests in the Institut d'Electronique, de Microélectronique et de Nanotechnologie, University of Lille 1, include the development of measurement techniques, the conception and realization of systems for microwave and millimeter-wave nondestructive evaluation purposes such as the characterization of nanodevices and electromagnetic wave interactions with different kind of materials (bulk, thin films, powders, etc).

Gilles Dambrine (M'-SM-F'17) was born in Avion, France, on May 15, 1959. He received the Ph.D. degree in 1989 and the Habilitation à Diriger des Recherches en Sciences degree in 1996, both from the Center Hyperfréquences et Semiconducteurs, University of Lille, Lille, France.

In 1986, he joined the Center Hyperfréquences et Semiconducteurs, University of Lille. From 1989 to 1999, he was a Full Researcher with the Center National de la Recherche Scientifique, Paris, France. He is currently a Professor of electronics with the University of Lille. He is also the Vice Deputy of the Institute of Electronics, Microelectronics, and Nanotechnologies (IEMN), Villeneuve d'Ascq, France, gathering about 500 researchers and Ph.D. holders. He is the Head of the Department of Micro, Nano, and Optoelectronics, IEMN. Over these few years, his research interests are oriented to the study of the microwave and millimeter wave properties and applications of nanodevices. He is an author or co-author of about 120 papers and communications and four chapters of books, in the field of microwave devices. His current research interests include modeling and characterization of ultimate low-noise devices for application in millimeter and sub-millimeter wave ranges. Dr. Dambrine is currently a reviewer of various IEEE Transactions and Letters. He is a member of the Technical Program Committee of the European EuMIC and ESSDERC conferences. He was the General Chair of the European Microwave Week 2010.

Chistophe Gaquière received the Ph.D. degree in electronic from the University of Lille, France, in 1995. He is currently Full Professor at the University of Lille (Polytech'Lille), and carries out his research activity at the Institut d'Electronique de Microélectronique et de Nanotechnology (IEMN). The topics concern design, fabrication, characterization and modeling of HEMT's and HBT devices. He works on GaAs, InP, metamorphic HEMT's and is currently involved in the GaN activities. His main activities are microwave characterizations (small and large signal between 1 and 500 GHz) to correlate the microwave performances with the technological and topology parameters. Today, his activities concern mainly the investigation of two-dimensional electronic plasmons and Gunn like effects for THz solid state GaN based detectors and emitters (HEMT and SSD), AlGaN/GaN nano-wires for microwave applications and MEMS activities based also on GaN. He was responsible for the microwave characterization part of the common laboratory between Thales TRT and IEMN focus on wide band gap semiconductor (GaN, SiC, and Diamond) from 2003 up to 2007. Now, he is in charge of the Silicon millimeter wave advanced technologies part of the common lab between ST microelectronics and IEMN. He is the author or co-author of more than 150 publications and 260 communications.